

## Site response at Yerba Buena Island, San Francisco Bay, California analyzed with weak motion recordings

L. BAISE<sup>(1)</sup>, L. HUTCHINGS<sup>(2)</sup> and S. GLASER<sup>(3)</sup>

<sup>(1)</sup> *Department of Civil and Environmental Engineering, Tufts University, Medford, Massachusetts, U.S.A.*

<sup>(2)</sup> *Hazards Mitigation Center, Lawrence Livermore National Laboratory, Livermore, California, U.S.A.*

<sup>(3)</sup> *Department of Civil and Environmental Engineering, University of California, Berkeley, California, U.S.A.*

(Received November 15, 2000; accepted November 22, 2001)

**Abstract** - We utilize weak motion recordings to evaluate the site response of Yerba Buena Island (YBI). YBI is a rock outcrop in San Francisco Bay, California, and is often used as a reference site in research and engineering studies. We identified 18 earthquakes in the area for which weak motion was recorded at the bottom and top of a 61-m borehole. Examining this data, we found that: (1) near-surface rock above the downhole site does not have a significant site response of its own; (2) there is a regional effect on seismic energy that severely attenuates frequencies above about 2 Hz. We suspect that this is due to propagation through the highly heterogeneous basement Franciscan formation. (3) Plots of the spectra for most of the recorded earthquakes show evidence for a spectral hole in the downhole recordings between 8 and 11 Hz as compared to the uphole recordings. We attribute this to interference between the up and downgoing waves. The downhole recordings would therefore cause a bias if used as a reference site without consideration of this interference. From these three observations, we conclude that at YBI the surface site provides the best recordings for reference rock sites or input into soils or engineering models. However, the effect of a regional site effect causing near-constant corner frequencies for recordings of  $M < 4.0$  earthquakes means that there is no true reference site, flat in spectral amplifications, available in the region. In this paper, we also compare site response and transfer function calculations using an auto-regressive moving average (ARMA) transfer function, and the horizontal-average, cross-spectra, complex signal, and horizontal-to-vertical spectral ratio methods. We found that the complex signal spectral ratio and ARMA transfer function calculations were more stable as

---

Corresponding author: Laurie Baise, Tufts University, 113 Anderson Hall, Medford, MA 02155 U.S.A.; phone: +6176272211; fax: +6176273994; e-mail: laurie.baise@tufts.edu

both site response calculations and as transfer functions. The horizontal-to-vertical method best revealed the lack of site response at YBI, and the calculation with just background noise gave as good results as that with seismic signal.

## 1. Introduction

We use a weak motion data set to examine the rock site response of Yerba Buena Island (YBI) in San Francisco Bay, California (Fig. 1). We further compare site response and transfer function calculations using five methods: the auto-regressive moving average (ARMA) transfer function and the horizontal-average, cross-spectra, complex-signal, and horizontal-to-vertical spectral ratio methods. We use recordings from the top and bottom of a 61m borehole in the analysis. We also evaluate the use of borehole recordings as reference sites and suggest the best method to create surface weak motion recordings from borehole recordings. In this paper we refer to site response in terms of spectral amplitudes, whereas transfer functions also include phase information.

The rock site response at YBI is a relevant issue for several reasons. First and foremost YBI is the middle anchor between the east and west spans of the San Francisco-Oakland Bay Bridge (SFOBB), the major east-west transportation artery in the San Francisco Bay Area. Second, the possibility that rock sites have a site response of their own (Margheriti et al., 1994; Cramer, 1995; Steidl et al., 1996; Archuleta et al., 2000) needs to be addressed for this site because it is often used as a reference site in research and engineering studies. In particular, YBI has been used as a reference site for several previous site response studies at Treasure Island (TI) for the M7.1 Loma Prieta earthquake, providing important evidence for nonlinear soil behavior (Jarpe et al., 1989; Idriss, 1990; Seed et al., 1991; Darragh and Shakal, 1991; Rollins et al., 1994). Third, it is centrally located in the San Francisco Bay borehole network (Hutchings, et al., 1999; Uhrhammer et al., 1999) and adjacent to the Treasure Island borehole array (Darragh and Shakal, 1991).

We use records of 18 earthquakes that occurred with a good range of magnitudes, distances, and azimuths and that were recorded at the bottom and top of the borehole. All data used in this study are from weak motion recordings ( $< 0.1$  g). Weak motion recordings offer the opportunity to utilize data that have propagation paths similar to that of large earthquake ground motion, that allow sampling in-situ soil properties, and that can be readily obtained in most seismically active regions. We do not address whether YBI site response will remain linear during strong ground motion.

The definition of site response or transfer functions is not uniformly accepted. In our view, ultimately, the best definition is that which provides a predictor of what will happen during future earthquakes. Site response or transfer functions represent the mapping of input ground motion at a reference site to output at another site. Site response or transfer functions should include the effects of softening geologic material, reverberations, or surface waves at a soil site that are not present at a reference site, or focusing and defocusing of energy at a rock site due to geologic structure or topography, but this may not be possible. Germane to this appoa-

ch is the assumption that at some basement depth all sites, locally, have a common wave propagation effect, and above this is the site response which can be described with a site response model.

The important constraint for the linear site response and transfer functions used herein and most commonly used in site response studies is that the output data (1) are linearly related to the changes in input amplitudes (amplitude linearity) and (2) remain constant for source spatial changes (phase linearity). Amplitude nonlinearity is a result of material (soil) softening or liquefying during high-amplitude shaking. There are many well-known codes that model amplitude nonlinearity (Schnabel et al. 1972; Prevost, 1993). Phase nonlinearity is a result of differences in wave propagation due to changes in source location. Phase nonlinearity cannot be modeled as a transfer function from a single point because energy enters the system from multiple points. For example, surface waves cannot generally be captured with linear ARMA or spectral ratio models because the surface wave energy is traveling horizontally and does not enter the system through the reference site. In order to constrain phase non-linearity, two- or three-dimensional waveform modeling is required (e.g. Larsen and Schultz, 1995). Empirical Green's functions can also be used to constrain phase non-linearity by identifying spatial dependence of waveforms. Hutchings and Wu (1990), for example, showed that small earthquakes located within about 2 km of each other and having the same focal mechanism preserve the phase for recordings of nearby stations and have near identical spectra when events are located as far as 15 km apart.

In this paper, site response calculated from uphole/downhole pairs will represent the mapping from downhole to uphole, relying on the assumption that the downhole site is representative of the local basement wavefield. Techniques typically used to obtain site response estimates from input/output pairs of ground motions include Fourier amplitude spectral ratios of single events (Borcherdt, 1970) and averaged values from a number of events (Jarpe et al., 1989; Blakeslee and Malin, 1991), cross-spectral ratios (Steidl, 1993; Safak, 1997), complex signal spectral ratios (Steidl, 1993; Tumarkin and Archuleta, 1997; and Tumarkin, 1998), coda spectral ratios (Aki, 1969; Malin, 1980). The horizontal-to-vertical spectral ratios (Nakamura, 1989; Field and Jacob, 1993; Lermo and Chavez-Garcia, 1993; Lachet and Bard, 1994; Bonilla et al., 1997) do not require a reference site for site response estimates. There is very little in the literature on extending these methods to obtain transfer functions. Bonilla et al. (1997) and Tumarkin and Archuleta (1997) discuss using the complex waveform and cross-spectral methods with phase preserved, respectively, but don't actually apply them. Methods such as system identification (Glaser, 1995; Baise and Glaser, 2000) and forward modeling, such as with SHAKE (Schnabel et al., 1972; Idriss, 1990) and SHAKE90 (Seed et al., 1991; Rollins et al., 1994) provide site response as well as transfer functions.

## 2. Geology of the study area

The San Francisco Bay Area is a seismically active region bordered on the east by the Hayward Fault and on the west by the San Andreas Fault (Fig. 1). YBI lies roughly midway

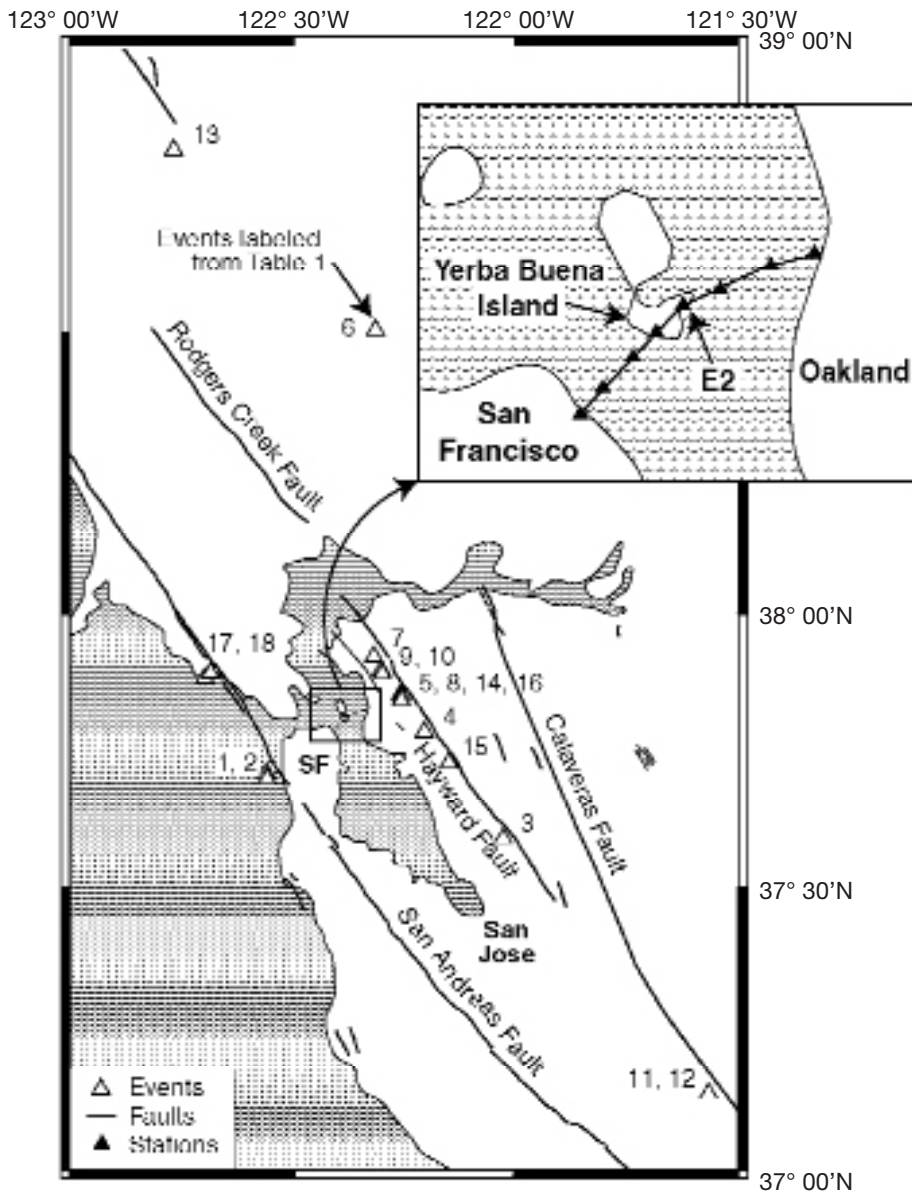


**Fig. 1** - Location of YBI, faults, and earthquake locations used in the study.

between these two important faults, a bedrock island in San Francisco Bay. The San Francisco Bay is a complex estuary that covers an area of 568 square kilometers, bounded on the east and west by parallel ranges of the northwest-trending Coast Ranges.

Much of the crust in this region is composed of the Franciscan formation from the Mesozoic Era, a highly fractured assemblage of rock. The Franciscan formation consists of interbedded feldspathic sandstone, graywacke, siltstone, shale, limestone, radiolarian chert, metavolcanic rocks, and glaucophane schists. The total thickness of this unit is unknown but has been estimated to be at least 10,000 feet thick and at most 50,000 feet thick. The Franciscan

material seismic velocities range from 4.3 to 6.1 km/s ( $V_p$ ) and are slightly lower in the upper 100 m. The uphole/downhole pair in this study is located in the Franciscan formation (Turpin, 2000).

Caltrans (1998) drilled and logged a borehole (# 94-9) near the instrumented E2 borehole site used herein. This log, plotted in Fig. 2, illustrates the geology from the surface to the bottom of the borehole. The material is predominantly graywacke interbedded with shale and siltstone. Vertical seismic profiles indicate that the shear-wave velocity varies from 3 km/s at 20 m depth to near 4.5 km/s from 28 to 52 m depth. The geology is essentially uniform throughout the borehole.

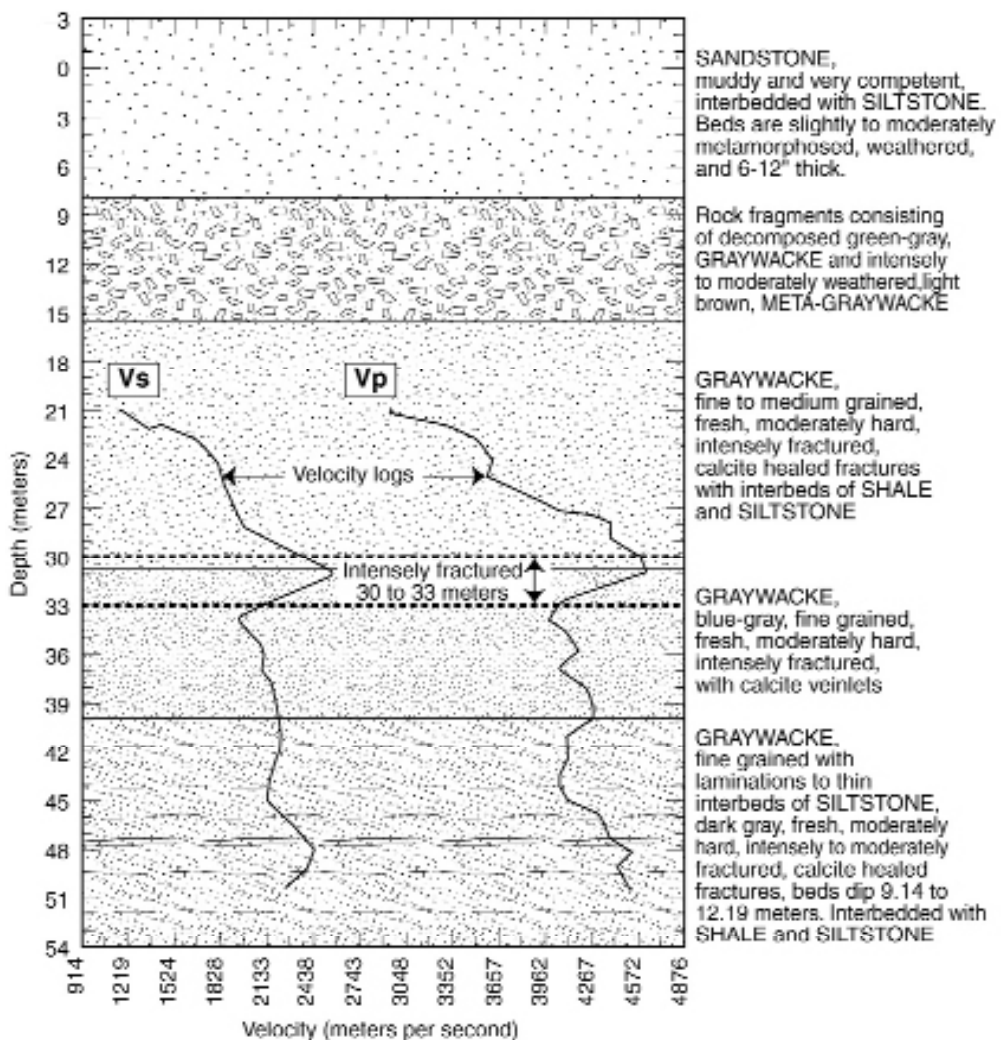


**Fig. 2** - Lithologic and velocity log for Caltrans boring 94-9, between Pier E1 and E2 on the Bay Bridge (near BE2D and BE2U).  $V_p$  and  $V_s$  in the figure refer to P-wave and S-wave velocities, respectively. Note the apparent contradiction of relatively high velocities coincident with highly fractured material at depths of 30 to 33 m.

### 3. Instrumentation and data

As a result of a collaboration between the Berkeley Seismographic Station Hayward Fault Network, Lawrence Livermore National Laboratory, Lawrence Berkeley National Laboratory, the U.S. Geological Survey, and Caltrans, a seismic network of six borehole and two surface instruments were installed along the SFOBB (Hutchings et al., 1999). Fig. 1 shows the location of the instruments. The surface recordings are at the San Francisco anchorage and the southern end of YBI. In addition, a temporary surface recorder was installed above the borehole on the east side of YBI above site E2. The borehole and surface recording at site E2 are analyzed in this paper. It is located at 37.8143 N, -122.3582 E. The uphole site is referred to as BE2U and the downhole site (at 61 m depth) is referred to as BE2D. We identified 18 events that were recorded on both the top and bottom of the borehole (Table 1). Locations and magnitudes listed in Table 1 are from the Northern California Earthquake Data Center (UCB, 2000). The locations of the 18 events are plotted in Fig. 1, and the magnitude range is from 1.9 to 5.0.

BE2U has a Reftek recorder and an S-6000 seismometer, and BE2D has a Quanterra recorder and Wilcoxon 731s 10v/g accelerometers. BE2D also contains three orthogonal Oyo HS-1, 4.5 Hz geophones for backup. The dynamic range of the Wilcoxon package is from a micro-g to 0.5 g acceleration and typically includes nearby microearthquakes greater than about  $M = 1.0$  as well as strong ground motion. The S-6000 clips at accelerations near 0.002 g, so we are limited to smaller or distant events at BE2U.

We have removed the response of each system to get ground motion to the frequency limit of the systems. The Wilcoxon accelerometers and Quanterra recorder (downhole system) are flat for acceleration from 0.1 Hz to the anti-alias filter at 100 Hz. The low-frequency limit is from a high-pass filter in the power box. It is down 3 db at 0.1 Hz and rolls off at 6 db per octave. The sensor has a roll-off at 0.05 Hz. The data were corrected for the 0.1 Hz high-pass filter, so the response is effectively flat to 0.05 Hz.

A portable Refraction Technology 72A Data Acquisition System with 16-bit resolution was used to record the S-6000 seismometer at BE2U. The Reftek recorder has a roll-off at 250 Hz and imposes an anti-aliasing filter at 40% of the sampling rate. We sampled the Reftek data at 200 sps, so it has a band limit of 80 Hz. The S-6000 seismometer is flat to velocity to at least 100 Hz and rolls off at the low frequency end; it is down 3 db at 2 Hz and rolls off at 12 db per octave. We have corrected for this high-pass filter, so that the response is effectively flat to DC.

Together, BE2D and BE2U have common data from 0.05 to 80 Hz. However, instrument and cultural noise further limit the effective frequency band of the data. Therefore, the signal-to-noise ratios (SNR) were calculated and evaluated to determine the usable frequency band of the data recorded for each earthquake as reported below. The downhole ground motions were recorded as accelerations and were therefore integrated to velocities to be consistent with the uphole recordings.

**Table 1** - Event Information and Spectral Parameters.

Earthquake	ID	Latitude	Longitude	<i>D</i>	<i>M</i>	data band BE2 U	data band BE2 D	<i>fa</i> BE2 U	<i>fa</i> BE2 D	<i>fh</i> BE2 D	Hypo Dist	Back Azm	Fault
1997/08/14 08:53	EV1+	37.737	-122.548	1.8	3.0	.6-40	.6-30	2	2	10	18.9	243	San Andreas
1997/10/27 14:30	EV2	37.727	-122.547	10.2	2.9	.7-60	2-10	6	6	-	21.8	240	San Andreas
1997/11/19 21:05	EV3+	37.619	-122.016	4.8	3.2	.3-40	1-30	4	4	13	37.5	211	Hayward
1998/01/17 10:00	EV4+	37.811	-122.193	4.5	2.4	.4-40	3-20	4	4	10	15.2	92	Hayward
1998/10/20 12:46	EV5	37.878	-122.246	10.0	2.1	.6-30	20-30	7	-	-	15.7	55	Hayward
1998/10/22 01:28	EV6	38.525	-122.303	8.3	3.0	.2-20	1-6	3	3	-	79.5	4	Lake Co.
1998/10/22 19:49	EV7	37.945	-122.307	7.6	2.5	.7-10	20-30	7	-	-	17.0	17	Hayward
1998/11/03 06:02	EV8	37.876	-122.243	9.5	2.4	.7-20	5-8	7	-	-	15.5	56	Hayward
1998/12/04 12:16	EV9+	37.920	-122.290	6.8	4.1	.7-40	.3-40	2	2	10	14.8	27	Hayward
1999/01/26 06:02	EV10	37.914	-122.288	4.7	2.0	1.3-7	NR	6	-	-	13.5	29	Hayward
1999/02/04 00:19	EV11+	37.160	-121.554	6.1	3.9	.3-20	.4-20	3	4	NH	101.8	136	Calaveras
1999/02/04 00:21	EV12+	37.161	-121.555	6.1	3.7	.5-15	.5-15	4	4	NH	101.7	136	Calaveras
1999/04/04 06:00	EV13	38.843	-122.757	4.0	3.8	.3-10	.4-8	3	3	-	119.5	343	Maacama
1999/06/23 23:48	EV14	37.874	-122.244	9.8	2.0	1 -30	5-8	4	-	-	15.5	57	Hayward
1999/07/24 05:28	EV15	37.756	-122.138	7.8	1.9	1.5-15	NR	4	-	-	21.9	109	Hayward
1999/08/12 08:16	EV16+	37.866	-122.245	6.5	2.5	.9-40	3-40	3	-	8	13.2	60	Hayward
1999/08/18 01:06*	EV17+	37.907	-122.687	6.7	5.0	.3-60	.3-60	1	1	10	31.4	289	San Andreas
1999/08/18 06:44	EV18	37.915	-122.674	7.2	2.6	.7-14	NR	4	-	-	30.8	292	San Andreas

\* clipped on the N310 component at BE2U  
 + used in spectral ratio study  
*D* is depth of event  
*M* is magnitude

NR no band had an acceptable ratio  
 NH no spectral hole identified  
*fa* is the corner frequency estimate from a Brune source model  
*fh* is the frequency of the spectral hole in the downhole component

**4. Data Analysis**

*4.1. Signal to noise ratios*

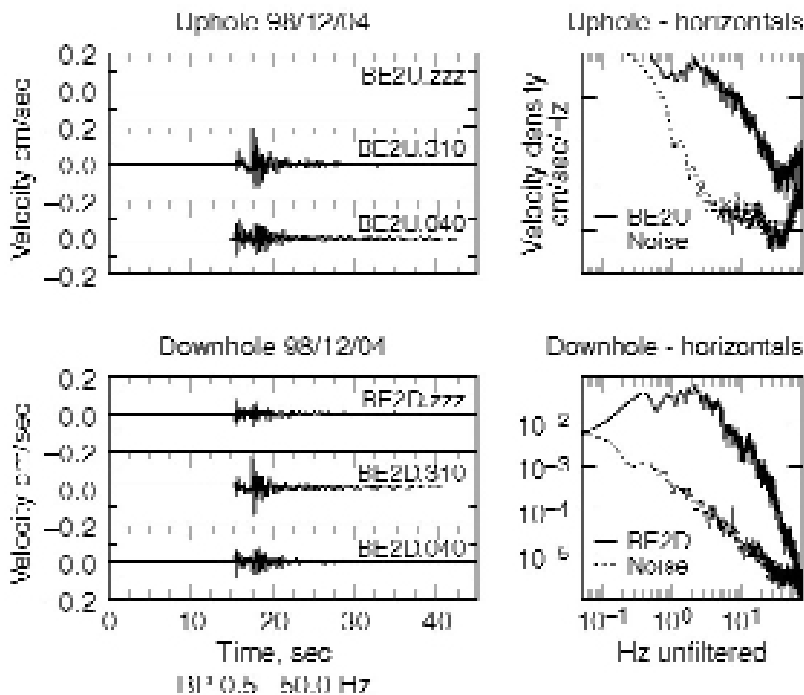
The SNR for each earthquake in this study is calculated by estimating the spectral content of the first 20 to 30 seconds of pre-event noise and a similar length of the earthquake signal (depending on the available length of the record). The two components of horizontal motion are

combined into a complex signal as described by Steidl et al. (1996). Fourier amplitude spectra of velocity records are used for the analysis. The Fourier signal amplitude spectrum is then divided by the Fourier noise spectrum for each earthquake. The SNR is calculated for the uphole and downhole recorded motions. A limiting SNR of 3:1 is chosen to define the usable frequency band of each signal. The usable frequency bands for the uphole and downhole ground motions are listed in Table 1.

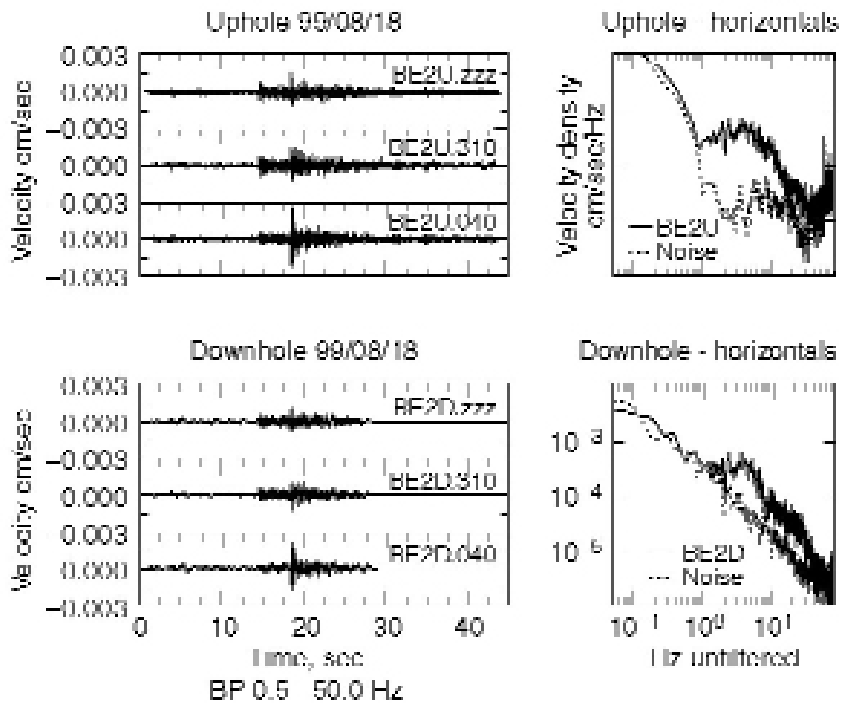
Fig. 3 shows the noise and signal spectra for both the uphole and downhole velocity recordings of EV9 (there is no vertical uphole recording for this event). This is a magnitude 4.1 earthquake at 15 km distance, one of the largest and closest recorded earthquakes, which demonstrates the high quality of data that can be recorded. The uphole and downhole recordings are limited by instrument noise at 0.3 Hz at the low frequency end, and at 40 Hz at the high frequency end.

Fig. 4 shows the velocity noise and signal spectra for both the uphole and downhole recordings of EV18. This magnitude 2.6 event is located 31 km away from YBI and is near the recording limit of the network. The uphole recording is limited to frequencies between 0.7 and 14.0 Hz and the downhole SNR is below 3 at all frequencies.

From Figs. 3 and 4 it is apparent that there is less noise at the surface site than the borehole site. The poor SNR at the downhole site is a result of instrument noise. The downhole site has strong-motion recording capacity but is limited for weak motion. The uphole instrument, on the other hand, is more adept at recording weak motion. This data set is not



**Fig. 3** - Time series and Fourier amplitude spectra for a magnitude 4.1 earthquake on the Hayward fault, 15 km distant. Noise spectra are also shown. The uphole and downhole recordings are limited at 0.3 Hz by instrument noise at the low frequency end, and at 40 Hz at the high frequency end, by cultural noise.



**Fig. 4** - Time series and Fourier amplitude spectra for a magnitude 2.6 earthquake recorded at the top and bottom of the borehole. Noise spectra are also shown. Cultural noise significantly reduces the usable frequency range.

appropriate for comparing the uphole versus downhole signal noise as a result of the different instruments. Examination of the noise and signal spectra for all 18 events in this study results in the following conclusions. The SNRs for the uphole recordings are generally greater than 3 over a frequency range of 0.5 to 30 Hz. The downhole recordings have a much smaller usable frequency range with SNR equal to or above 3, from 1 to 8 Hz. However, the usable frequency range varies over the recorded earthquakes. Examination of the SNR confirms that 13 events are usable between 1 and 10 Hz, whereas only 8 of the events are good over this range for the downhole recordings.

#### 4.2. Corner frequency

When spectra are plotted for events of differing magnitudes, the corner frequency is expected to vary directly with magnitude. This is not the case for the spectra at YBI. Rather, most of the spectra show apparent corner frequencies between 2 and 7 Hz, regardless of magnitude. Table 1 lists apparent spectral corner frequencies ( $f_a$ ) picked by eye for all the events with the appropriate usable frequency band. Apparent corner frequencies may be a result of the source, propagation path, or site effect. Fig. 5, shows spectra from EV8 and EV12 with magnitude 2.4 and 3.7, respectively. The picked corner frequencies are 6 and 5 Hz, respectively, as indicated in the figure. Even though EV12 has a much larger magnitude and greater distance than EV8, the corner frequencies are about the same.

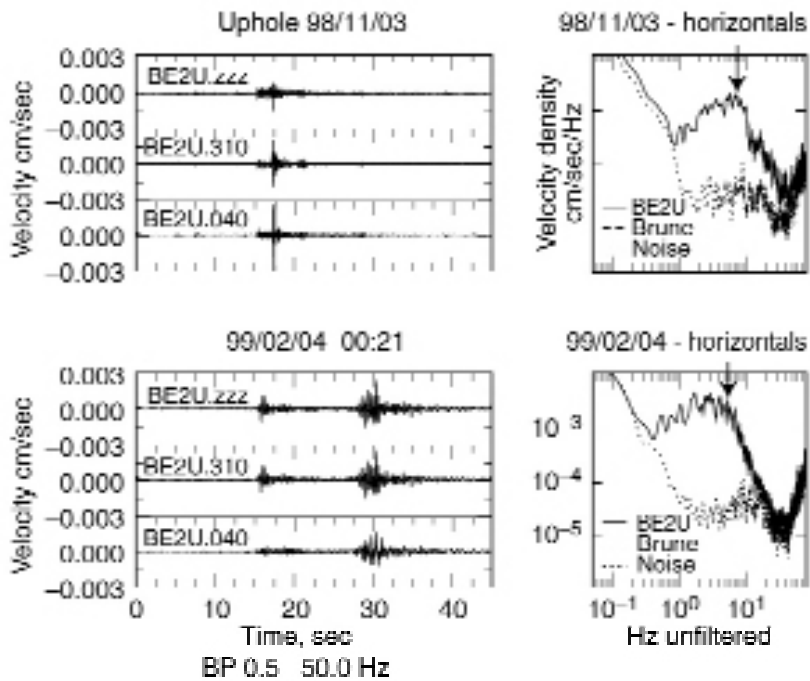


**Fig. 5** - Time series and Fourier amplitude spectra for a magnitude 2.4 (top) and a magnitude 3.7 (bottom) earthquake recorded at the top of the borehole. Notice the similarity of the shape of the spectra. The corner frequencies fit by eye are 6 and 5 Hz, respectively. Even though the  $M = 3.7$  event is much larger and occurred at a greater distance than the  $M = 2.4$  event, the corner frequencies are about the same.

Fig. 6 shows a plot of the corner frequency picks (triangles) as a function of moment (using the moment magnitude relation of Bakun, 1984), along with the predicted corner frequencies using a Brune (1971) source model, stress drop of 100 bars, and source shear velocity of 3.0 km/s. Only events with moment above about  $1.0 \times 10^{21}$  dyne-cm (EV9,

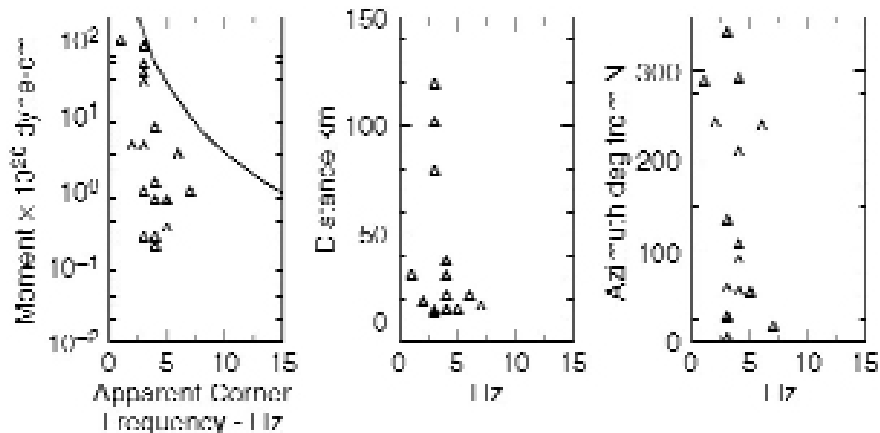


**Fig. 6** - Plots of moment (left), distance (center), and azimuth (right) as a function of corner frequency for all the events listed in Table 1. Also shown is the prediction of corner frequencies with a Brune (1972) source model (left) with stress drop of 100 bars. Only events with moment greater than  $1.0 \times 10^{21}$  dyne-cm have a corner frequency near the predicted.

EV17, EV11) have corner frequencies near what would be expected from a Brune source model.

As discussed in the literature, the constant corner frequencies could be explained several ways: as a source effect, as a site effect, or as a path effect. First the source effect: there could be a breakdown of the constant stress drop Brune source model that calls for corner frequencies to increase with decreasing magnitude. Several authors have identified constant corner frequencies for small events and attributed these to a minimum source dimension for earthquakes, which results in a decrease in stress drop for smaller events (Archuleta et al., 1982; Papageorgiou and Aki, 1983). However, a wide body of literature has refuted the explanation of the constant corner frequency observed for small earthquakes as being a source effect (Anderson and Hough, 1984; Hutchings and Wu, 1990; Aster and Shearer, 1991; Blakeslee and Malin, 1991; Abercrombie, 1995).

Second, regarding the local site effect: the local geology at YBI could cause amplification between 2 and 7 Hz, or cause high attenuation at frequencies above about 2 Hz; both of which would give the appearance of a corner frequency. The possibility of a local YBI site effect is investigated by picking corner frequencies at other stations in the region. Table 2 lists other rock sites in San Francisco Bay that recorded events listed in Table 1, and their distance from the events. The sites are borehole sensors 100 feet in bedrock along the Bay Bridge (Hutchings et al., 1999). Stations YBA, W05, W02, and SFA are progressively farther west of BE2U, and stations BE07 and BE17 are progressively farther east of BE2U (Fig. 1). It is apparent from Table 2, with limited data, that the low corner frequencies observed at BE2U and BE2D are also recorded at other nearby rock sites. This suggests that a site-specific effect at YBI is not likely the cause of the constant corner frequency; however, a more regional site effect could be possible. Each of these stations is in the Franciscan material beneath the San Francisco Bay.

An alternative explanation is that the constant low corner frequencies result from high whole path attenuation removing the high frequencies from the signals uniformly over the various

**Table 2** - Corner frequencies at rock sites in San Francisco Bay.

Earthquake	STA	<i>f<sub>a</sub></i>	dist. (km)
1997/11/19 21:05	BE2U	4	37.1
	W05	4	37.7
1998/01/17 10:00	BE2U	4	15.2
	BE07	4	14.3
	BE17	4	13.4
	BW02	5	17.6
	BW05	3	16.6
1998/10/20 12:46	BE2U	5	15.7
	BE17	5	14.2
1998/12/04 12:16	BE2U	3	14.8
	BE07	2	14.1
	BE17	2	13.5
	SFA	9	18.5
	YBA	3	15.5
	BW02	2	17.9
	BW05	2	16.6

events. A whole path Q effect would be greater for larger hypocentral distances; therefore, the corner frequencies are plotted against hypocentral distance in Fig. 6. Corner frequencies versus event azimuth are also plotted in Fig. 6. As evident from the figure, a relationship between hypocentral distance or azimuth and corner frequency does not appear to exist.

In summary, the source, site, and whole-path effects do not seem to cause the near-constant corner frequencies. We suspect that constant corner frequencies are due to attenuation caused by propagation through the highly heterogeneous basement Franciscan formation beneath the recording sites in the San Francisco Bay. Several studies have shown that corner frequency estimates from surface recordings are limited to a maximum value due to near-site attenuation (Hanks, 1982; Anderson and Hough, 1984; Hutchings and Wu, 1990; Hutchings, 1991). In one such study, Hutchings (1991) plotted spectra of aftershocks, with magnitudes near 3.0, of the Loma Prieta earthquake recorded at YBI and found a constant corner frequency near 5 Hz. In the present study, the magnitude range is increased to include a M5.0 and M4.1 event with similar results. The M4.1 event has a corner frequency of 2 Hz, and the M5.0 event has a corner frequency of 1 Hz, both matching the expected Brune source corner and indicating that with these increased magnitudes the expected source corner is below the maximum value allowed by regional site attenuation. Further study is required to fully resolve the issue.

#### *4.3. Uphole versus downhole*

Another question addressed in this study was to determine the differences between surface and borehole rock recordings with respect to rock site response and use as a reference site. As previously discussed, the recorded ground motions are affected by the differences in SNR for the uphole and downhole recordings as a result of the different instruments. Also, the apparent corner frequency is observed equally in the uphole and downhole ground motion spectra. In terms of site response, a rock reference site should have a flat spectral response with no amplification, in order not to bias the soil site response calculation or transfer functions.

Plots of the signal spectra for the eight recorded earthquakes with an appropriate usable frequency band show evidence for a spectral hole in the downhole recordings between 8 and 11 Hz as compared to the uphole recordings. The uphole spectra are smooth with a constant slope through this frequency range. The spectral hole is identified by a loss of energy over the frequency band, or rather an indent in otherwise smooth spectra. The spectral hole varies in width and depth over the earthquakes in this study but is consistently observed for all but two earthquakes. Fig. 7 shows the calculated Fourier spectra for the uphole and downhole recordings of EV9 with the spectral hole indicated. For a two-way travel time of the surface reflection (120 m total), and an assumed shear wave velocity of 1 km/s, a spectral hole would be expected around 9 Hz. The two earthquakes that do not exhibit a spectral hole near 9 Hz in the downhole recordings occur at large epicentral distances (all over 100 km). As a result of the long travel path, most of the high frequency energy has been attenuated, and the incident angle is very shallow. Either of these issues may explain the lack of an observed spectral hole.

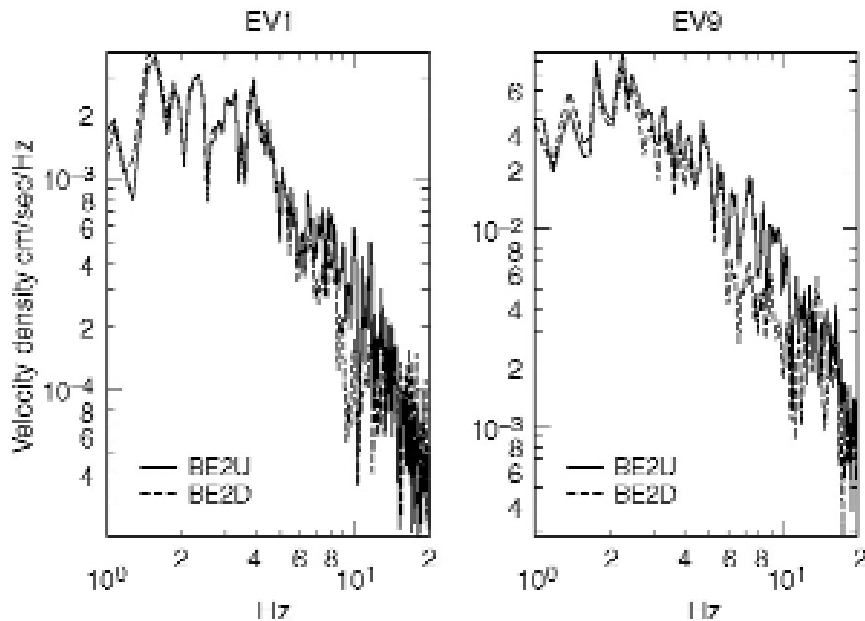


**Fig. 7** - Fourier amplitude spectra for up- and downhole pairs of horizontal records (N310E) for events EV1 and EV9 that show the spectral hole near 8 Hz for the downhole records (dotted line).

## 5. YBI site response and transfer functions

Site response and transfer functions are estimated by using the borehole as a reference site. Five available methods are used: system identification with ARMA models, and horizontal-average, cross-spectral, complex-signal, and horizontal-to-vertical spectral ratio methods. Results of this effort are used to further analyze the rock site response at YBI. Each of the above methods are used with the eight available uphole/downhole event pairs (identified with a + in Table 1) to develop a site response and transfer function estimate. The methods are tested by predicting surface spectra and time histories from borehole recordings. Inherent in this approach is the assumption that the borehole site represents the input signal. Because the input motion has a spectral hole as a result of wavefield interference, it does not in itself represent the regional bedrock motion but rather the specific bedrock motion of the instrument location and therefore can represent the input to the overlying system. Therefore, the spectral hole between 7 and 10 Hz will not affect the evaluation here because we are only testing how well the functions predict the recorded output observation given an input, and the input does not need to meet the criteria of a true reference site to test this.

Correlation of uphole/downhole pairs is used to assess the quality of the data used for estimating linear transfer functions (Baise, 2000). Input/output waveform pairs need to be linearly correlated in order to estimate reliable linear transfer functions and all the methods used herein are linear transfer function methods (Bendat and Piersol, 1980). The correlation coefficient used herein is the maximum value of the cross-correlation of two waveforms. This definition provides for a propagation lag between stations. The correlation coefficients for the

two horizontal components are averaged to a single value. Based on the calculated correlation between uphole and downhole waveforms, the eight events are highly correlated ( $r > 0.90$ ). Using all 18 unfiltered events, there exists a noticeable decline in correlation of uphole/downhole pairs for events with magnitudes less than 3.0. Above  $M = 3.0$ , the events are all highly correlated ( $r > 0.90$ ). A quadratic trend-line fit to the data highlights this systematic relationship between low correlation and low magnitude in Fig. 8. To determine if the low correlation for the small events is a result of low SNR, the data is filtered over a passband from 1 to 10 Hz. This passband is chosen to isolate the high SNR portion of the signal. The calculated correlation coefficients also exhibit a similar trend but to a lesser extent. For events with  $M > 3.0$ , the correlation coefficients are relatively constant, indicating that above this magnitude the data is coherent.

Each of the site response/transfer function methods is evaluated using a series of goodness-of-fit measures. In the time domain, a peak error statistic and a normalized mean square error are implemented. The normalized mean square error (*NMSE*) takes into account the non-stationarity of earthquake ground motions by windowing the data to contain all peaks with amplitudes greater than 0.2 of the maximum value, the peak ground motion or *PGM* (Baise, 2000). The resulting mean square error is also normalized by the peak value to allow for comparison between events and by the digital-sampling rate. The *NMSE* is therefore calculated according to:

$$NMSE = \frac{1}{b-a} \sum_{t=a}^b \left( \frac{y}{PGM} - \frac{\hat{y}}{PGM} \right)^2, \tag{1}$$

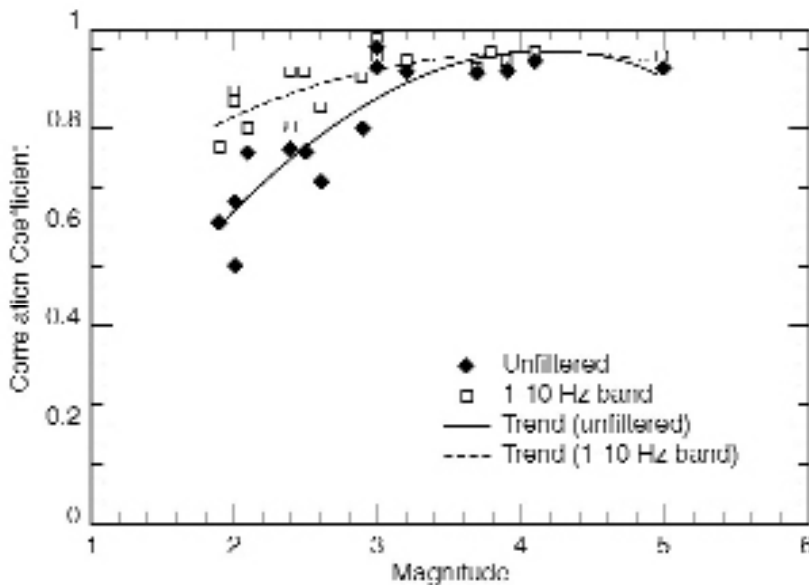


**Fig. 8** - Correlation coefficients for the uphole/downhole pairs at YBI plotted against magnitude for events listed in Table 1. A quadratic polynomial trend line is shown for both the unfiltered uphole/downhole pairs and the pairs filtered to a 1-10 Hz passband (removing effect of low SNR).

where  $y$  is the observed time series,  $\hat{y}$  is the predicted time series and  $a$  and  $b$  are the limits of the time series including all amplitudes greater than 0.2 of the  $PGM$ . The peak amplitudes are compared using a peak error statistic ( $PES$ ):

$$PES = \frac{|\max |y| - \max |\hat{y}| |}{\max |y|} = \frac{|PGM(y) - PGM(\hat{y})|}{|PGM(y)|} \tag{2}$$

Finally, the spectral fit error is averaged and the standard deviation calculated.

### 5.1. System identification and ARMA transfer functions

Using a system identification framework, an auto-regressive moving average (ARMA) transfer function for the YBI site is estimated from uphole/downhole waveform pairs according to Baise (2000) and Baise and Glaser (2000). This approach has the added benefit of being valid when only a single earthquake is used for the estimate, whereas spectral ratios require an ensemble estimate to reduce variance. In order to assess the advantage of using this single earthquake method and to assess the consistency of the resulting transfer function estimates, three transfer function estimates are made from three of the available events: EV3, EV9, and EV17.

The largest events recorded at the YBI vertical array are EV9 ( $M = 4.1$ ) and EV17 ( $M = 5.0$ ), which were used to estimate transfer functions. The ground motions at the surface and in the borehole are highly coherent (0.93 for EV9 and 0.92 for EV17). Again, this high degree of correlation indicates that the ground motions from the surface and the downhole location can be linearly related, and the estimated linear transfer function should be reliable. In addition, EV3 ( $M = 3.2$ ) is estimated to provide an example of the reliability of a lower magnitude event transfer function. Fig. 9 provides an indication of the variability of the three

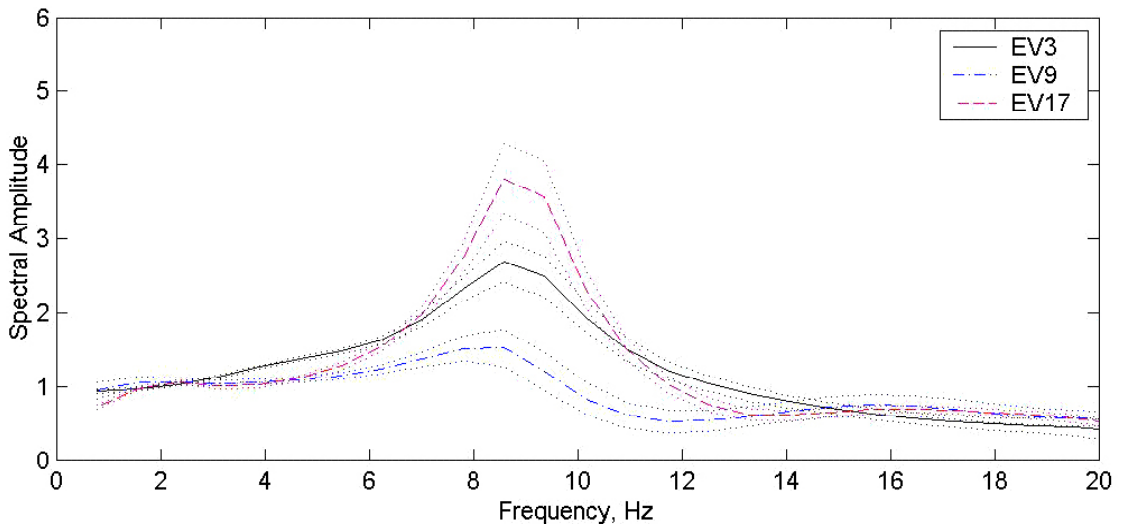


**Fig. 9** - Comparison of three ARMA transfer functions estimated at BE2 for EV3, EV9, and EV17. Each transfer function is plotted with 95% confidence intervals shown as dotted lines.

estimated transfer functions which are plotted with the 95% confidence intervals. The transfer functions estimated from the three events differ in peak amplitudes but only slightly in peak location. The EV17 estimate has the highest peak (maximum amplitude = 3.7) centered at 9 Hz, whereas the EV9 estimate peaks at amplitude 1.4 at 8.5 Hz and EV3 peaks at 2.6 at 9 Hz. Therefore, the location of the peak is well defined but not the amplitude. This result is consistent with theory as discussed by Gersch (1974).

The reliability of each transfer function model is tested by using it to predict the uphole ground motions for the eight events given the downhole recording. The accuracy of these predictions are quantified with the *NMSE* and secondly with a *PES*. These error statistics are summarized in Table 3. The ARMA transfer function estimated for EV9 shown in Fig. 10a, b is relatively flat with a broad peak between 6 and 11 Hz with amplification near 2. The 95% confidence intervals shown in the figure indicate an uncertainty in the amplification from 3 to 4.5. The motions recorded at BE2U for EV17 are plotted against those predicted by the EV9 ARMA model given the BE2D input motion in Fig. 10c. The model-simulated waveforms are 14% low at the peak, indicating that the model is not capturing all of the amplification in the data. The corresponding spectra are plotted in Fig. 10d. The model-simulated spectra follows the shape of the recorded motion to 7 Hz and then indicates an amplification in the simulation from 8 to 10 Hz, not observed in the recorded data. This result indicates that the ARMA transfer function may be over-compensating for the apparent spectral hole amplification. The simulated spectra are also below the recorded spectra above 12 Hz where the transfer function is below 1. The low transfer function value in this range is most likely a result of the low energy (as well as low SNR) in this frequency range.

### 5.2. Spectral ratio methods

Site response and transfer functions from the bottom to the top of the borehole are also obtained by the horizontal-average, cross-spectral, complex-representation, and horizontal-to-vertical spectral ratio methods. For site response functions, only the Fourier amplitude spectra were used, and comparisons were in the frequency domain. Transfer functions also include phase relations, and comparisons were made in the time and frequency domain. Transfer functions that assumed zero-phase shift are also tested. Figs. 11, 12, 13, and 14 show exam-

**Table 3** - Error analysis for transfer function estimates (*NMSE*, *PES* and Spectral *MSE*).

	<i>NMSE</i> (phase)	<i>NMSE</i> (zero phase)	<i>PES</i>	Spectral <i>MSE</i>
ARMA transfer function EV9	0.028		18.5%	
ARMA transfer function EV17	0.013		20 %	
ARMA transfer function EV3	0.0093		14 %	
Horizontal Average Spectral Ratio	0.225	0.069		0.003
Cross-spectra Spectral Ratio	0.216	0.059		0.003
Complex Spectral Ratio	0.115	0.035		0.003

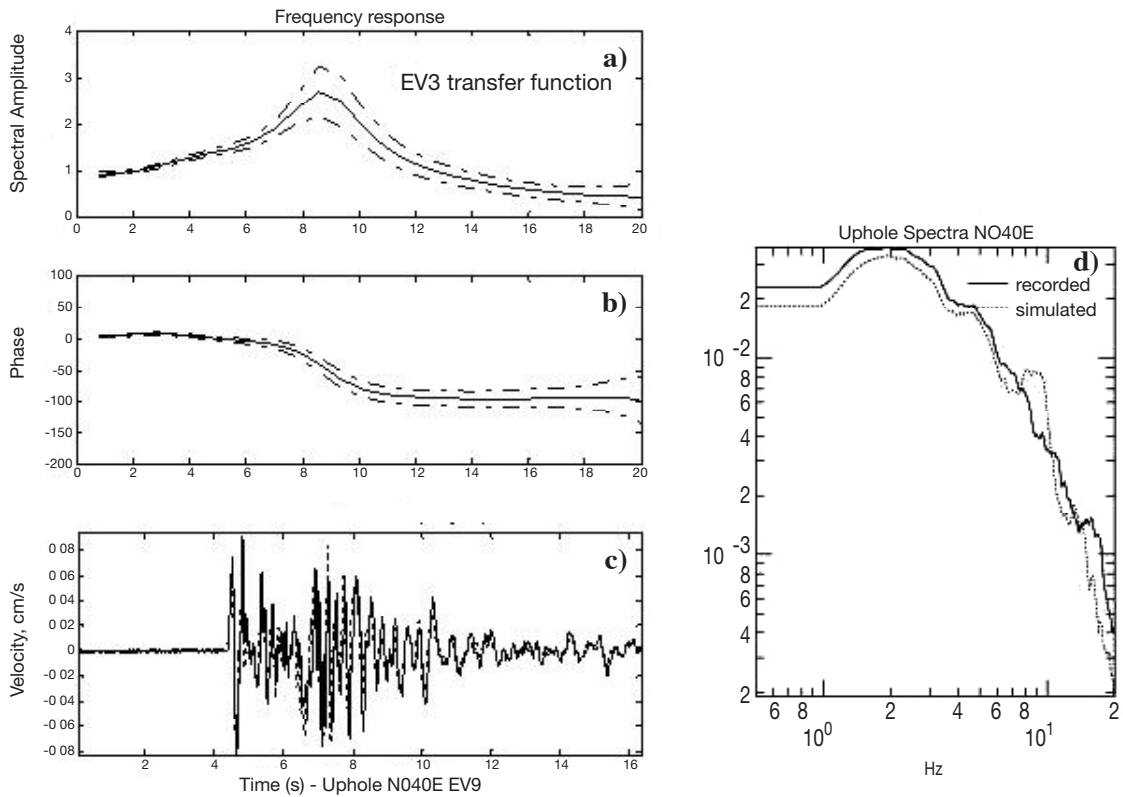


**Fig. 10** - (a, b) Estimated ARMA site response transfer function and corresponding phase for EV3 plotted with 95% confidence intervals. (c) Observed and simulated (dashed line) surface motion for the (EV9) N040E component using the observed downhole motion as input and the EV3 transfer function. (d) Corresponding observed and simulated spectra.

ples for the four methods. Two predicted time series are shown for each method, one from a calculated phase spectrum and one assuming zero-phase shifts for the transfer function. The basic assumption of the spectral ratio methods (except horizontal-to-vertical) is that travel paths and source effects will be the same for both sites so that the spectral ratios will show the amplification and phase shifts between the bottom and top of the borehole. Only horizontal components are used (except for horizontal-to-vertical). In the following discussion, consider two horizontal components ( $X_1, X_2$ ) to be recorded at the surface and two horizontal components ( $Y_1, Y_2$ ) to be recorded from the same event at the bottom of the borehole. The orientation of the recordings are assumed known unless otherwise specified.

The Fourier transforms of the two horizontal components for the up- and down-hole records are:  $F \{X_1\} = A_1 - iB_1$ ,  $F \{X_2\} = A_2 - iB_2$ ,  $F \{Y_1\} = C_1 - iD_1$ , and  $F \{Y_2\} = C_2 - iD_2$ , respectively. The right-hand side of each equation is a function of frequency, as are each of the following equations. Details of Fourier analysis can be found in many time series analysis textbooks. In the following, details such as instrument response, propagation path effects, and effect of noise are ignored; they have been discussed in many previous studies, such as Steidl (1993), Bonilla et al. (1997) and Safak (1997).

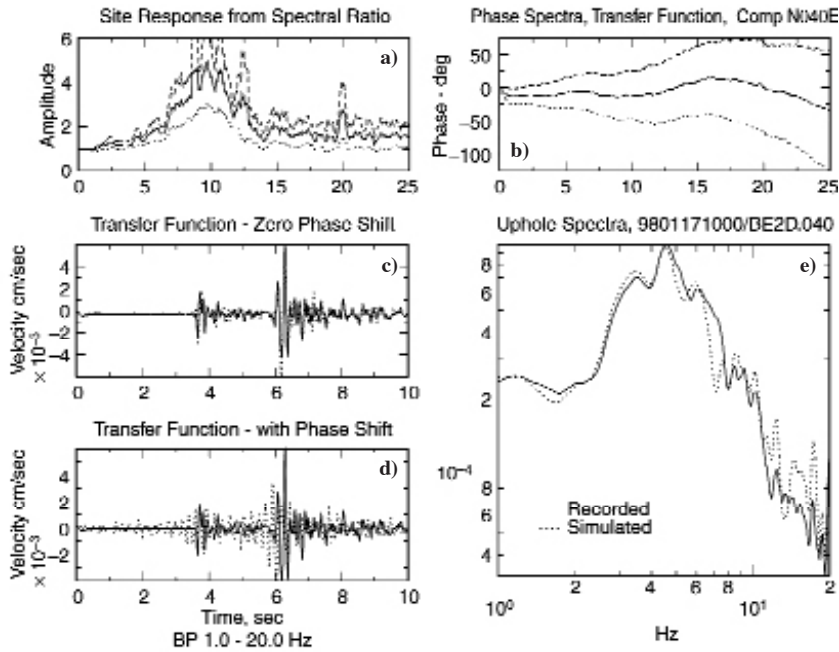


**Fig. 11** - (a, b) Estimated horizontal-average site response function for eight events plotted with 95% confidence intervals. (c) Observed and simulated surface motion for EV4, N040E component, using the observed downhole motion as input and zero phase shift in the transfer function. (d) Using phase in the transfer function. (e) Corresponding observed and simulated spectra.

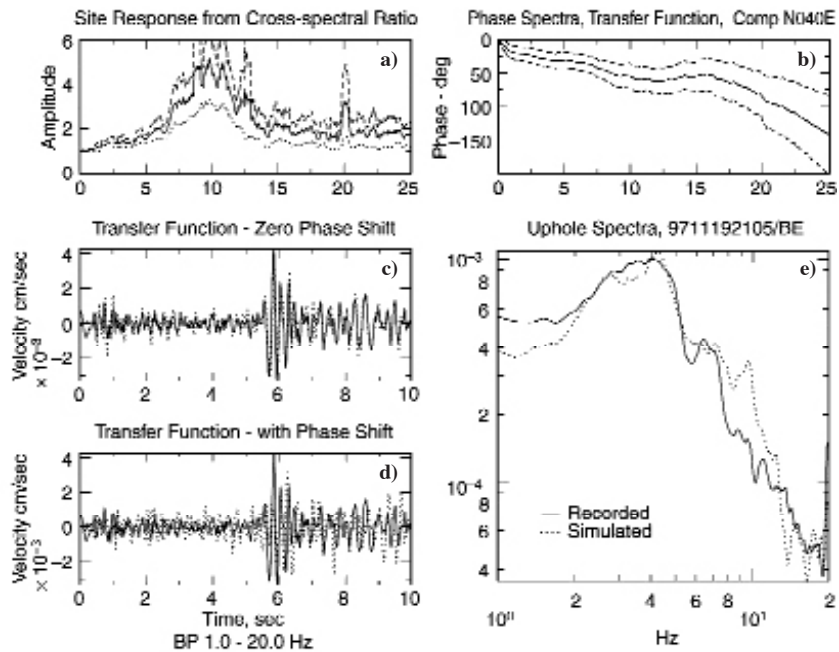


**Fig. 12** - (a, b) Estimated cross-spectra site response function for eight events plotted with 95% confidence intervals. (c) Observed and simulated surface motion for EV3, N040E component, using the observed downhole motion as input and zero phase shift in the transfer function. (d) Using phase in the transfer function. (e) Corresponding observed and simulated spectra.

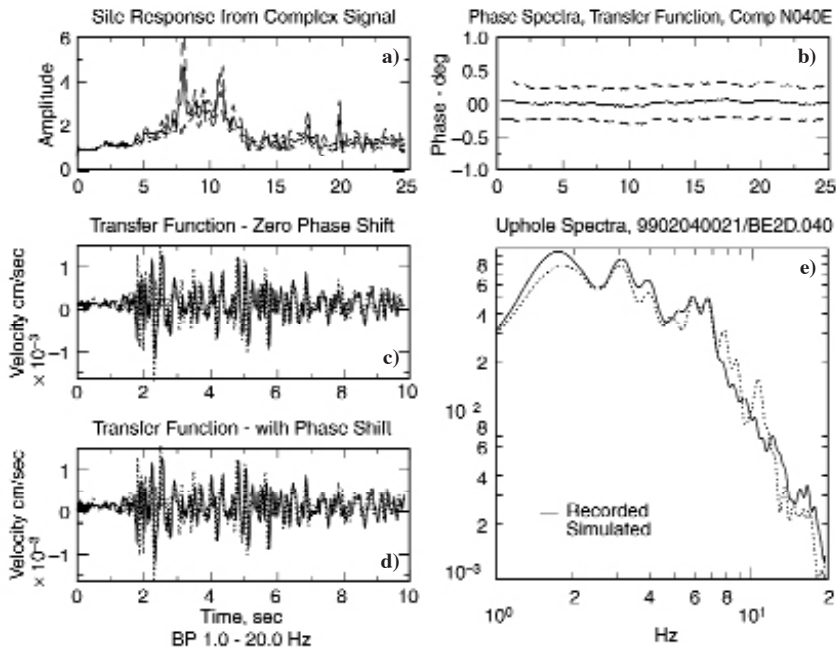


**Fig. 13** - (a, b) Estimated complex-signal site response function for eight events plotted with 95% confidence intervals. (c) Observed and simulated surface motion for EV12, N040E component, using the observed downhole motion as input and zero phase shift in the transfer function. (d) Using phase in the transfer function. (e) Corresponding observed and simulated spectra.

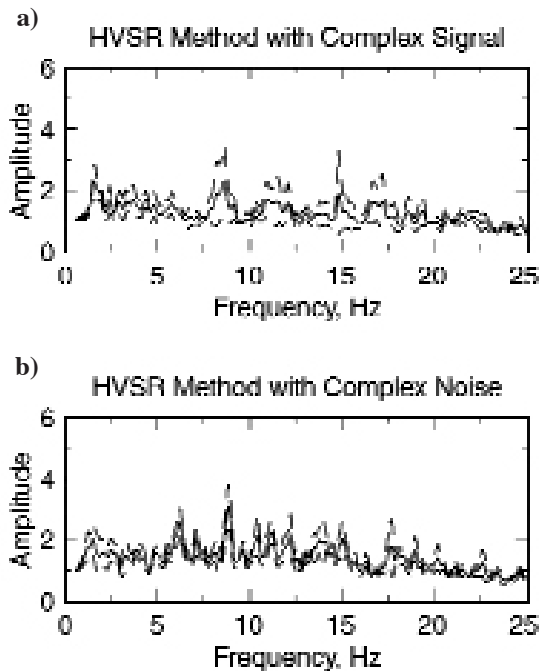


**Fig. 14** - Horizontal-to-vertical spectral ratio using the complex signal for the horizontal components. Mean and plus and minus one standard deviation are shown. (a) Seismic signals from eight events are used in this calculation. (b) Pre-event noise from records of eight events is used in the calculation.

The horizontal-average spectral ratio is found by first obtaining the ratio of individual components:

$$R_1 = \frac{A_1 - iB_1}{C_1 - iD_1} \quad \text{and} \quad R_2 = \frac{A_2 - iB_2}{C_2 - iD_2}. \quad (3)$$

With amplitude spectra:

$$|R_1| = \frac{\sqrt{A_1^2 + B_1^2}}{\sqrt{C_1^2 + D_1^2}} \quad \text{and} \quad |R_2| = \frac{\sqrt{A_2^2 + B_2^2}}{\sqrt{C_2^2 + D_2^2}}, \quad (4)$$

and with phase spectrum:

$$P_1 = \text{atan} \left( \frac{A_1 D_1 + B_1 C_1}{A_1 C_1 + B_1 D_1} \right) \quad \text{and} \quad P_2 = \text{atan} \left( \frac{A_2 D_2 + B_2 C_2}{A_2 C_2 + B_2 D_2} \right). \quad (5)$$

So that the horizontal-average spectral ratio amplitude spectra is:  $|R| = \frac{|R_1| + |R_2|}{2}$ , and the phase is:  $|P| = \frac{|P_1| + |P_2|}{2}$ . The phase spectra are unwrapped when combined.

Fig. 11 shows the estimated horizontal-average site response function for eight events plotted with the 95% confidence intervals, and observed and simulated surface motions with and without phase for EV4 using the recorded downhole motion as input. Also shown are corresponding observed and simulated spectra. The up- and down-hole records have been rotated to the same orientation, and the spectral ratio for each horizontal component is calculated separately, averaged and smoothed; then, those for all eight events were averaged. The optimum results were obtained with a smoothing window of 0.24 Hz or less. It is apparent that the transfer function with zero phase shifts provides the best results. The *NMSEs* for the time series from predicting all eight events average to 0.225 and 0.069, for simulations with phase and without phase respectively. The spectral *MSE* average is 0.003.

The cross-spectral ratio is found by multiplying the numerator and denominator of the spectral ratio by the conjugate of the denominator:

$$R_1 = \frac{(A_1 - iB_1)(C_1 - iD_1)}{C_1^2 + D_1^2} \quad \text{and} \quad R_2 = \frac{(A_2 - iB_2)(C_2 - iD_2)}{C_2^2 + D_2^2}. \quad (6)$$

With amplitude spectra:

$$|R_1| = \frac{\sqrt{(A_1 C_1 + B_1 D_1)^2 + (B_1 C_1 - A_1 D_1)^2}}{\sqrt{C_1^2 + D_1^2}} \quad (7)$$

and

$$|R_2| = \frac{\sqrt{(A_2 C_2 + B_2 D_2)^2 + (B_2 C_2 - A_2 D_2)^2}}{\sqrt{C_2^2 + D_2^2}} \quad (8)$$

and with phase spectrum:

$$P_1 = \text{atan} \left( \frac{A_1 D_1 + B_1 C_1}{A_1 C_1 + B_1 D_1} \right) \quad \text{and} \quad P_2 = \text{atan} \left( \frac{A_2 D_2 + B_2 C_2}{A_2 C_2 + B_2 D_2} \right), \quad (9)$$

the same as for the spectral ratio method.

So the horizontal-average spectral ratio amplitude spectra is:  $|R| = \frac{|R_1| + |R_2|}{2}$ , and the phase  $P = \frac{P_1 + P_2}{2}$ . The phase spectra are unwrapped when combined.

Fig. 12 shows the estimated cross-spectral site response function averaged for eight events plotted with 95% confidence intervals, and observed and simulated surface motions with and without phase for EV3 using the recorded downhole motion as input. Also shown are corresponding observed and simulated spectra. The up- and down-hole records have been rotated to the same orientation, and the cross-spectral ratio for each horizontal component is calculated separately, averaged, and smoothed; then, those for all eight events were averaged. The optimum results were obtained with a smoothing window of 0.24 Hz or less. It is apparent that the transfer function with zero phase shifts gives the best results. The *NMSEs* for the time series from predicting all eight events average to 0.216 and 0.059 for simulations with and without phase, respectively. The spectral *MSE* average is 0.003. The cross-spectral ratio amplitude spectrum has slightly larger standard deviation than the spectral ratio results, but the phase spectrum has significantly smaller standard deviation values.

The complex representation spectral ratio is found by first combining the time series for each site to create a two-dimensional time series:  $X = X_1 + iX_2$  and  $Y = Y_1 + iY_2$ , where  $X_1$  and  $X_2$  are the horizontal components of the uphole recordings and  $Y_1$  and  $Y_2$  are the horizontal components of the downhole recordings. The spectral ratio then is:

$$R = \frac{F\{X_1 + iX_2\}}{F\{Y_1 + iY_2\}} = \frac{(A_1 + B_2) - i(B_1 - A_2)}{(C_1 - D_2) - i(D_1 - C_2)}. \quad (10)$$

The amplitude and phase spectrum are easily obtained by solving the arithmetic to get  $R$  into its real and imaginary parts and applying the usual relations. The phase spectrum of such a time series is a complicated combination of the phases of the horizontal components and has no apparent physical significance. Tumarkin (1998) points out that unlike Fourier transforms of real time series, which have conjugate complex values at symmetric frequencies, complex Fourier transforms have non-symmetric values at symmetric frequencies.

Fig. 13 shows estimated complex-representation site response function averaged for eight events plotted with 95% confidence intervals, and observed and simulated surface motions with and without phase for EV12 using the recorded downhole motion as input. Also shown are corresponding observed and simulated spectra. There is no need to know the orientation of the two sites in this method. The optimum results were obtained with a smoothing window of 0.24 Hz or less. The transfer function with zero phase shifts gives better results than those with phase

included. The *NMSEs* for the time series from predicting all eight events average to 0.115 and 0.035, respectively. The spectral *MSE* average is 0.003.

The horizontal-to-vertical spectral ratio assumes that the P and S-waves are vertically propagating and that the P-waves are not affected by the geology (Mucciarelli and Gallipoli, 2001). It is calculated by:

$$R = \frac{F\{X_1 + iX_2\}}{\sqrt{2} F\{X_3\}} = \frac{(A_1 + B_2) - i(B_1 - A_2)}{\sqrt{2} (A_3 - iB_3)} . \quad (11)$$

Where, again, the amplitude and phase spectrum are easily obtained by solving the arithmetic to get *R* into its real and imaginary parts and applying the usual relations. The horizontals are combined into a complex spectra as was done for the complex representation spectral ratio, and identified as the best approach by Bard (1999).  $X_3$  is the vertical component of the horizontal record, and the factor of two is from the maximum amplitude factor and the patrician of energy factor (Lachet and Bard, 1994).

Fig. 14a shows the horizontal-to-vertical spectral ratio of eight events along with 95% confidence intervals. No attempt is made to use this as a transfer function to predict the uphole records since the reference site in this case has a spectral hole. The site response obtained in this way is nearly one over the broad frequency band. Fig. 14b shows the horizontal-to-vertical spectral ratio of pre-event noise from records of the eight events. It is apparent that both these spectral ratios show no site effect at YBI and that the solution with only background noise gives as good results as the solution with seismic signal.

From examination of the *NMSE* summarized in Table 3, it is apparent that the ARMA and complex-representation method with zero phase shift give the best results. The complex-representation has a benefit of simplicity and lack of need for knowing the orientation of the downhole record. The ARMA method can be achieved with only one event. We conclude that the best method to create surface weak motion recordings from borehole recordings is either with the ARMA transfer function or the complex-signal spectral ratio without phase.

It is also apparent from Figs. 11 through 13 that the site response is flat and near one for frequencies outside the band of the spectral hole. This suggests that there is no near-surface site response. The horizontal-to-vertical spectral ratio apparently shows this very well, and doesn't have the effect of the spectral hole in its site response estimation.

## 6. Conclusions

In summary, we set out to identify the site response at YBI. We have concluded that the event corner frequencies are relatively constant between 2 and 7 Hz from magnitude 1.9 to 4.1. Only for the M4.1 and M5.0 events are the corners consistent with the Brune source model. This result is consistent with previous investigations indicating further evidence for a regional attenuation effect through the heterogeneous Franciscan formation. The rock site response identified with uphole/downhole transfer functions was consistent for spectral ratios and ARMA

transfer functions and identified a flat response with the exception of a peak between 8 and 12 Hz consistent with wavefield interference in the downhole recording. For the YBI site, the surface station provides a more reliable reference site since there is little evidence for a rock site response and the downhole recording is hindered by the spectral hole near 9 Hz. In this case, the horizontal-to-vertical spectral ratio is highly uncertain and does not provide a consistent site response estimate. In terms of a comparison of methods, the ARMA transfer functions provide an estimate of the site response, which is similar in accuracy to the spectral ratio methods but at a significantly lower cost (single event). Each of the methods resulted in a slightly different estimate of the amplification at the peak but the peak location was consistently identified at 9 Hz.

We found that: (1) near-surface rock above the downhole site does not have a significant site response of its own; (2) there is a regional effect on seismic energy that severely attenuates frequencies above about 2 Hz. We suspect that this is due to propagation through the highly heterogeneous basement Franciscan formation. (3) Plots of the spectra for most of the recorded earthquakes show evidence for a spectral hole in the downhole recordings between 8 and 11 Hz as compared to the uphole recordings. We attribute this to interference between the up and downgoing waves. The downhole recordings would therefore cause a bias if used as a reference site without consideration of this interference. From these three observations, we conclude that at YBI the surface site provides the best recordings for reference rock sites or input into soils or engineering models. However, the effect of a regional site effect causing near-constant corner frequencies for recordings of  $M < 4.0$  earthquakes means that there is no true reference site, flat in spectral amplifications, available in the region.

**Acknowledgments.** We benefited from reviews by Lucia Margheriti and an anonymous reviewer. We also benefited from discussions with Paul Kasameyer, Alexei Tumarkin and Jamie Steidl. Cindy Hayek provided surface geologic descriptions and operated the surface recorder. This project was partially supported by the Lawrence Livermore National Laboratory, Campus/Laboratory Collaboration Project, and under the auspices of the US Department of Energy by the University of California, under contract No. W-7405-Eng-48. It was partially funded by Caltrans under contract no. 59A0238 for site response analysis.

## References

- Abercrombie R.E.; 1995: *Earthquake source scaling relationships from -1 to 5 ML using seismograms recorded at 2.5 km depth*. J. Geophys. Res., **100**, 24015 - 24036.
- Archuleta R.J., Cranswick E., Mueller C. and Spudich P.; 1982: *Source parameters of the 1980 Mammoth Lakes, California, earthquake sequence*. J. Geophys. Res., **87**, 4595-4608.
- Aki K.; 1969: *Analysis of the seismic coda of local earthquakes as scattered waves*. J. Geophys. Res., **74**, 615-631.
- Anderson J.G. and Hough S.; 1984: *A model for the shape of the Fourier amplitude spectra of accelerograms at high frequencies*. Bull. Seis. Soc. Am., **74**, 1969-1994.
- Archuleta R., Steidl J.H. and Bonilla L.F.; 2000: *Engineering insights from data recorded on vertical arrays*. In: 12th World Conference in Earthquake Engineering, Auckland, New Zealand, 7 pp., CD-ROM.

- Archuleta R.J., Cranswick E., Mueller C. and Spudich P.; 1982: *Source parameters of the 1980 Mammoth Lakes, California, earthquake sequence*. J. Geophys. Res., **87**, 4595-4608.
- Aster R.C. and Shearer P.M.; 1991: *High-frequency borehole seismograms recorded in the San Jacinto fault zone, southern California. 2. Attenuation and site effects*. Bull. Seis. Soc. Am., **81**, 1081-1100.
- Baise L.G.; 2000: *Investigations in site response from ground motions observations in vertical arrays*. Ph.D. Dissertation, University of California, Berkeley.
- Baise L.G. and Glaser S.D.; 2000: *Consistency of ground-motion estimates made using system identification*. Bull. Seis. Soc. Am., **90**, 993-1009.
- Bakun W.H.; 1984: *Seismic moments, local magnitudes, and coda-duration magnitudes for earthquakes in central California*. Bull. Seis. Soc. Am., **74**, 439-458.
- Bard P.-Y.; 1999: *Microtremor measurements: A tool for site effect estimation?* In: Irikura K., Kudo K., Okada H. and Sasatani T. (eds), *The Effects of Surface Geology on Seismic Motion*. Balkema Rotterdam, pp. 1251-1279.
- Bendat J.S. and Piersol A.G.; 1986: *Engineering applications of correlation and spectral analysis*, John Wiley & Sons, Inc., New York, 566 pp.
- Blakeslee S. and Malin P.; 1991: *High-frequency site effects at two Parkfield downhole and surface stations*. Bull. Seis. Soc. Am., **81**, 332-345.
- Bonilla L.F., Steidl J.H., Lindley G.T., Tumarkin A.G. and Archuleta R.J.; 1997: *Site amplification in the San Fernando valley, CA: variability of the site effect estimation using the S-wave coda, and H/V methods*. Bull. Seis. Soc. Am., **87**, 710-730.
- Borcherdt R.D.; 1970: *Effects of local geology on ground motion near San Francisco Bay*. Bull. Seis. Soc. Am., **60**, 29-61.
- Brune J.N.; 1971: *Tectonic stress and the spectra of seismic shear waves from earthquakes*. J. Geophys. Res. **75**, 4997-5010 (Correction, J. Geophys. Res. **76** (20), 5002, 1972).
- Caltrans; 1998: *SFOBB East Span Seismic Safety Project 30% Type Selection, May 29*. Fugro-EMI Project No. 98-42-0035.
- Cramer C.H.; 1995: *Weak-motion observations and modeling for the Turkey Flat, U.S., site-effects test area near Parkfield, California*. Bull. Seism. Soc. Am., **85**, 440-451.
- Darragh R.B. and Shakal A.F.; 1991: *The site response of two rock and soil station pairs to strong and weak ground motion*. Bull. Seism. Soc. Am., **81**, 1885-1899.
- Field E.H. and Jacob K.H.; 1993: *The theoretical response of sedimentary layers to ambient seismic noise*. Geophysical Research Letters, **20**, 2925-2928.
- Gersch W.; 1974: *On the achievable accuracy of structural system parameter estimates*. Journal of Sound and Vibration, **34**, 63-79.
- Glaser S.D.; 1995: *System identification and its applications to estimating soil properties*. J. of Geotech. Eng., ASCE, **121**, 553-560.
- Hanks T.C.; 1982:  $f^{max}$ . Bull. Seis. Soc. Am., **72**, 1867-1879.
- Hutchings L.; 1991: *"Prediction" of strong ground motion for the 1989 Loma Prieta earthquake using empirical Green's functions*. Bull. Seis. Soc. Am., **81**, 88-121.
- Hutchings L. and Wu F.; 1990: *Empirical Green's functions from small earthquakes: a waveform study of locally recorded aftershocks of the San Fernando earthquake*. J. Geophys. Res., **95**, 1187-1214.
- Hutchings L., Kasameyer P., Foxall W., Hollfelder J., Turpin C., Hayek C., Uhrhammer R. and Jarpe S.; 1999: *Deep borehole instrumentation along San Francisco Bay bridges - 1999*. Lawrence Livermore National Laboratory, UCRL 132137.
- Idriss I.M.; 1990: *Response of soft soils during earthquakes*. In: Duncan J.M. (ed), *H. Bolton Seed Memorial Symposium*, Vol. 2, BiTech Publishers Ltd., Vancouver, B.C., Canada, pp. 273-289.

- Jarpe S.J., Hutchings L.J., Hauk T.F. and Shakel A.F.; 1989: *Selected strong- and weak-motion data from the Loma Prieta earthquake sequence*. Seism. Res. Lett., **60**, 167-176.
- Lachet C. and Bard P.-Y.; 1994: *Numerical and theoretical investigations on the possibilities of Nakamura's technique*. J. Phys. Earth, **42**, 377-397.
- Larsen S.C. and Schultz C.A.; 1995: *ELAS3D: 2D/3D elastic finite-difference wave propagation code*. Technical Report No. UCRL-MA-121792, 18 pp.
- Lermo J. and Chavez-Garcia F.; 1993: *Site effect evaluation using spectral ratios with only one station*. Bull. Seism. Soc. Am., **83**, 1574-1594.
- Malin P.E.; 1980: *A first-order scattering solution for modeling elastic waves codas. I. The acoustic case*. Geophys. J. R. Astr. Soc., **63**, 361-380.
- Margheriti L., Wennererg L. and Boatwright J.; 1994: *A comparison of coda and S wave spectral ratios as estimates of site response in the southern San Francisco Bay area*. Bull. Seism. Soc. Am., **84**, 1815-1830.
- Nakamura Y.; 1989: *A method for dynamic characteristics estimation of subsurface using microtremors on the ground surface*. Quart. Rev. Rail. Trans. Res. Inst. (RTRI), **30**, 25-33.
- Papageorgiou A.S. and Aki K.; 1983: *A specific barrier model for the quantitative description of inhomogeneous faulting and the prediction of strong ground motion, I, Description of the model*. Bull. Seis. Soc. Am., **73**, 693-722.
- Prevost J.H.; 1993: *"DYNFLOW User's Manual"*. Princeton University Civil Eng.
- Rollins K.M., Mchood M.D., Hryciw R.D. and Homolka M.; 1994: *Ground response on Treasure Island*. Strong Ground Motion, A109-A121.
- Safak E.; 1997: *Models and methods to characterize site amplification from a pair of records*. Earthquake Spectra, **13**, 97-129.
- Schnabel P., Seed H.B. and Lysmer J.; 1972: *SHAKE: A computer program for earthquake response analysis of horizontally layered sites*. Report No. UCB/EERC-72/12, Earthquake Engineering Center, University of California, Berkeley.
- Seed R.B., Dickenson S.E. and Idriss I.M.; 1991: *Principal geotechnical aspects of the 1989 Loma Prieta earthquake*. Soils and Foundations, **31**, 1-26.
- Steidl J.; 1993: *Variation of site response at the UCSB dense array of portable accelerometers*. Earthquake Spectra, **9**, 289-302.
- Steidl J.H., Tumarkin A.G. and Archuleta R.J.; 1996: *What is a reference site?* Bull. Seis. Soc. Am., **86**, 1733-1748.
- Tumarkin A.G. and Archuleta R.J.; 1997: *Recent advances in prediction and processing of strong motions*. Natural Hazards, **15**, 199-215.
- Tumarkin A.G.; 1998: *Site response analysis in 3d*. In: Irikura K., Kudo K., Okada H., Sasatani T. (eds), *The Effects of Surface Geology on Seismic Motion*. Vol. I, Balkema, Rotterdam, pp. 365-370.
- Turpin C.; 2000: *Seismic profile of the Franciscan Formation beneath the San Francisco-Oakland Bay bridge*. San Francisco Bay, California, senior thesis, California State University, Sacramento, California.
- UCB; 2000: *Northern California Earthquake Data Center* <http://quake.geo.berkeley.edu/ncedc/ncedc.access.html>.
- Uhrhammer R., Romanowicz B., Dreger D., Neuhauser D., McEvilly T. and Clymer R.; 1999: *Annual Report 1998-1999*. UC Berkeley Seismographic Station.

